Analysis for the Progressive Failure Response of Textile Composite Fuselage Frames

Final Report — Summary of Research

Eric R. Johnson
Principal Investigator

Performance Period: 10 June 2001 to 31 July 2002

NASA Grant NAG-1-01123

Aerospace and Ocean Engineering Department
Virginia Polytechnic Institute and State University
Blacksburg, Virginia 24061-0203

July 31, 2002

Technical Officer: Dr. Richard L. Boitnott, Mail Stop 495
National Aeronautics and Space Administration
Langley Research Center
Hampton, Virginia 23681-2199

Introduction

A part of aviation accident mitigation is a crashworthy airframe structure, and an important measure of merit for a crashworthy structure is the amount of kinetic energy that can be absorbed in the crush of the structure. Prediction of the energy absorbed from finite element analyses requires modeling the progressive failure sequence. Progressive failure modes may include material degradation, fracture and crack growth, and buckling and collapse. The design of crashworthy airframe components will benefit from progressive failure analyses that have been validated by tests.

The subject of this research is the development of a progressive failure analysis for a textile composite, circumferential fuselage frame subjected to a quasi-static, crash-type load. The test data for the frame are reported in Ref. 1, and these data are used to develop and to validate methods for the progressive failure response.

Circumferential Frame Specimens and Tests

The structural components tested in Ref. 1 were the size of a typical circumferential fuselage frame for a wide body commercial transport aircraft with a nominal inside radius of 118 inches and a radial depth of 4.8 inches. The frame segments are 48° circular arcs with an asymmetrical cross section in the shape of the letter *J*. A detailed illustration of a frame denoted as *B* along with its dimensions is shown in Fig. 1.

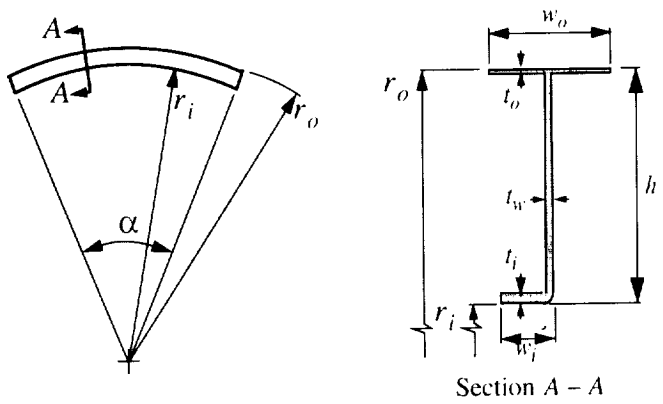

w_i, in.	1.25
w_o, in.	2.77
t_i, in.	0.204
t_o, in.	0.0885
t_w, in.	0.159
h, in.	4.80
r_i, in.	117.85
r_o, in.	122.65
α, degrees	47.21

Figure 1 J-section fuselage frame B

The frames were fabricated from 2X2 2-D triaxial braided textile composite preforms coupled with the resin transfer molding process using 3M PR500 epoxy resin. The architecture of the preforms is $[0°_{18k}/\pm 64°_{6k}]$ 39.7% axial, and the yarns are made of AS4 graphite fibers. Material property data are listed in Table 1.

Table 1. Tri-axial braid properties for V_f = 55.26%

Properties	TEXCAD[2]	Tension Tests[3]
Axial modulus E_{11}, psi	7.06×10^6	7.09×10^6
Transverse modulus E_{22}, psi	6.59×10^6	N/A
Thickness modulus E_{33}, psi	1.53×10^6	N/A
Poisson's ratio (ν_{12})	0.231	0.26
Poisson's ratio (ν_{13})	0.216	N/A
Poisson's ratio (ν_{23})	0.298	N/A
In-plane shear modulus G_{12}, psi	1.91×10^6	N/A
Transverse shear modulus G_{13}, psi	0.601×10^6	N/A
Transverse shear modulus G_{23}, psi	0.645×10^6	N/A
Tensile failure strain ($\varepsilon_1'^{T}$, $\mu\varepsilon$)	14,071	10,588
Compression failure strain ($\varepsilon_1'^{C}$, $\mu\varepsilon$)	10,108	N/A
Axial tensile strength X_T, psi	91,370	76,880
Axial compressive strength X_C, psi	71,000	N/A
Transverse tensile strength Y_T, psi	73,140	N/A
Transverse compressive strength Y_C, psi	56,890	N/A
In-plane shear strength S, psi	30,460	N/A

A sketch of the frame mounted in a universal testing machine is shown Figure 2. The structural testing consisted of mounting frame *B* vertically, convex side up, in a universal testing machine and subjecting it to a slowly applied, radially inward displacement at its apex. In addition to in-plane bending and circumferential compression, the asymmetric *J*-section frame exhibits out-of-plane bending and torsion. The largest circumferential strain magnitude was compressive and occurred in the outer flange at the apex. A compressive hoop strain of approximately one-half this maximum value occurred in the inner flange near the supported ends of the frame. The largest circumferential tensile strains are much less than the largest compressive strain magnitudes. The maximum compressive strain recorded at the first major failure event is about 4000 $\mu\varepsilon$ which is substantially less than the material ultimate compression strain of 10,108 $\mu\varepsilon$ predicted by TEXCAD[2] computer program for this material system.

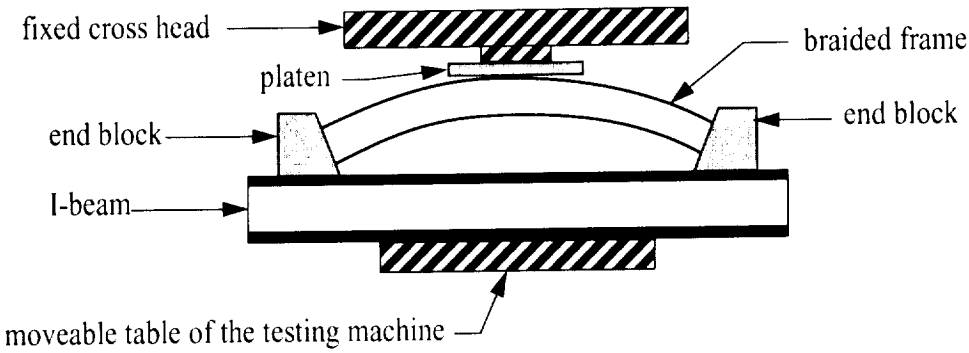

Figure 2 Sketch of the frame test apparatus

Frame *B* Progressive Failure Analysis

Finite element models of frame *B* were developed in the ABAQUS/Standard software package[4] using the dimensions listed in Figure 1, the material property data listed in Table 1, and using the finite-membrane-strain shell elements available in ABAQUS. Clamped boundary conditions were prescribed in the analyses to simulated the frame mounted in the end blocks. To simulate the contact of the platen with the frame, we used a contact algorithm available in ABAQUS. A rigid plane parallel to the platen was displaced in the downward direction into the outer flange of the frame.

Intralaminar Failure and Degradation

A FORTRAN subroutine was written to be used in conjunction with ABAQUS to predict intralaminar failure initiation followed by a degradation in the moduli. The algorithm follows one used in Ref. 5 for intralamina progressive failure of a unidirectional composite material. The in-plane strengths for the triaxial braid determined from TEXCAD are listed in Table 1. With this limited material strength data, we assumed a maximum in-plane stress criterion to predict the initiation of failure in an element. The FORTRAN subroutine used is called from the ABAQUS input deck under the *USER DEFINED FIELD command. The state of stress in an element from the equilibrium state at the previous load is passed to the subroutine prior to the next load increment. The in-plane stresses are compared to their corresponding strengths. If the stress magnitudes equal or exceed their corresponding strengths, then the value of a field variable is changed from zero to one. Field variables are a means to indicate whether failure has occurred or has not occurred; a value of zero means no failure and a value of one means failure. The values of the field variables are returned to the input deck where they are used to determine which lines of material properties are used to calculate the stress and strains for the next load step.

The maximum in-plane stress criterion is non-interactive and is based on the values of the axial normal stress S_{11}, the transverse normal stress S_{22}, and the in-plane shear stress S_{12}. Consequently three field variables are required: Field variable $FV1$ is associated with the axial normal stress limits, $FV2$ is associated with the transverse normal stress limits, and field variable $FV3$ is associated with the shear stress limits. The initial values of the three field variables are zero, representing an intact layer. If $S_{11} \geq 91.37\text{ksi}$ or $S_{11} \leq -71\text{ksi}$, then $FV1 = 1$ and the axial modulus (E_{11}) is multiplied by a factor of $1/10^6$ and the transverse modulus (E_{22}) and the shear moduli (G_{12}, G_{13}, G_{23}) are multiplied by a factor of 1/1000. If $S_{22} \geq 73.14\text{ksi}$ or $S_{22} \leq -56.89\text{ksi}$, then $FV2 = 1$, and the same scheme as used before is followed but the transverse modulus (E_{22}) is multiplied by a factor of $1/10^6$ and the axial

modulus (E_{11}) is multiplied by a factor of 1/1000. If $|S_{12}| \geq 30.46$ksi , then $FV3 = 1$ and the in-plane moduli (E_{11}, E_{22}) and the out of plane shear moduli (G_{13}, G_{23}) are multiplied by a factor of 1/1000, the in-plane shear modulus (G_{12}) is multiplied by a factor of $1/10^6$. For combinations of failure modes, the previous reduction factors are combined together decreasing each property by the largest factor unless the factors are equal and greater than $1/10^6$. In the latter case, there is an additional reduction of 10. For example, if the values of field variables are (1,0,1), which indicates a combination of axial and shear failure, then E_{11} and G_{12} are decreased by $1/10^6$ and E_{22}, G_{13}, G_{23} are multiplied by $1/10^4$ because the axial failure factor is $1/10^3$ and the shear failure factor is $1/10^3$. See Table 2 for the property degradation scheme.

Table 2. Reduction Factors For Intralaminar Material Degradation

ABAQUS field variables			Reduction Factor for Each Material Property								
FV1	FV2	FV3	E_{11}	E_{22}	E_{33}	ν_{12}	ν_{13}	ν_{23}	G_{12}	G_{13}	G_{23}
0	0	0	1	1	1	1	1	1	1	1	1
1	0	0	$1/10^6$	$1/10^3$	1	0	0	0	$1/10^3$	$1/10^3$	$1/10^3$
0	1	0	$1/10^3$	$1/10^6$	1	0	0	0	$1/10^3$	$1/10^3$	$1/10^3$
0	0	1	$1/10^3$	$1/10^3$	1	0	0	0	$1/10^6$	$1/10^3$	$1/10^3$
1	1	0	$1/10^6$	$1/10^6$	1	0	0	0	$1/10^4$	$1/10^4$	$1/10^4$
1	0	1	$1/10^6$	$1/10^4$	1	0	0	0	$1/10^6$	$1/10^4$	$1/10^4$
0	1	1	$1/10^4$	$1/10^6$	1	0	0	0	$1/10^6$	$1/10^4$	$1/10^4$
1	1	1	$1/10^6$	$1/10^6$	$1/10^3$	0	0	0	$1/10^6$	$1/10^5$	$1/10^4$

Delamination Initiation and Progression

Interface elements are used to model the delamination process between adjacent layers of the quasi-laminar textile composite. The interface element used to model interlaminar crack initiation and growth in tape laminates developed by Goyal, Johnson, Dávila, and Jaunky[6] was implemented in the finite element analysis (FEA) of the frame. Interface elements were located in the models at the mid surface of the outer flange, where delamination was observed to initiate in the tests. The displacements of the sublayers above and below the mid plane where the interface elements are located determine interlaminar tractions through a phenomenological constitutive law. Each interface element consists of two surfaces and eight nodes, an upper and lower surface with four nodes each. The four nodes on the upper surface of the interface element connect to the four nodes on the lower surface of the element in the upper sublayer of the outer flange. The four nodes on the lower surface of the interface element connect to the four nodes on the upper surface of the element in the lower sublayer of the flange. In the undeformed state the two surfaces of the interface element coincide. The constitutive law that resists the separation of the upper and lower surfaces of the interface element can be conceptualized as representing a continuous distribution of nonlinear springs that do not interact with one another; i.e. similar to Winkler foundation. A graphical representation of the interface element is shown in Figure 3.

The constitutive law relates the tractions to the displacement jumps across the interface. An exponential form of the this relationship is used in Ref. 6, which is illustrated for Mode I loading, the opening mode, in Figure 4. In this figure T is the traction, Δ is the displacement jump normal to the interface, T^o is the specified tensile, or peel, strength, and G_c is the specified critical strain energy release rate in Mode I. Tractions first increase with increasing Δ, reach a maximum at $\Delta = \Delta_c$, then decrease as $\Delta > \Delta_c$. The exponential form of the law and specification of T^o and G_c determine the critical separation length $\Delta = \Delta_c$. The critical separation length is a characteristic length scale for the initiation of two free surfaces of the incipient crack. The softening portion of the constitutive law represents

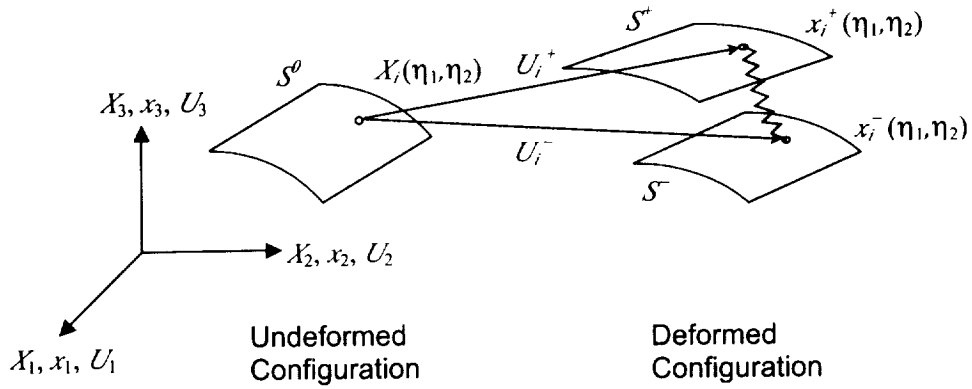

Figure 3 Upper (S^+) and lower (S^-) surfaces of the interface element.

the presence of the process zone ahead of the crack tip, which is a craze zone in polymers or a plastic zone in ductile metals. Under combined Mode I, II, and III loading, delamination initiation is predicted using multi-axial stress criterion and the propagation of delamination is based on an mixed-mode fracture criterion[6]. A damage parameter is included in the formulation such that on unloading from a state where $\Delta > \Delta_c$, the traction does not follow the loading curve. That is, unloading is associated with a loss of work.

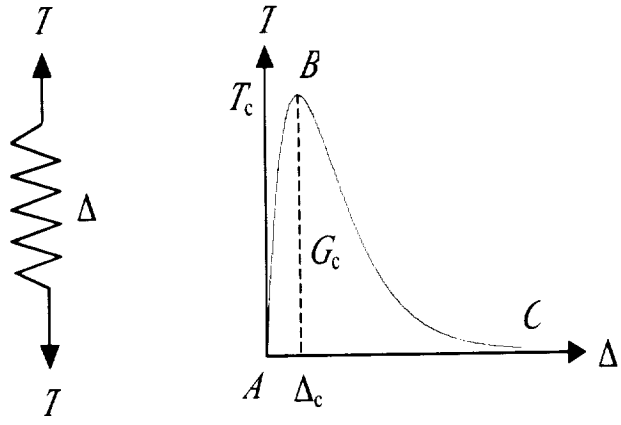

Figure 4 Representative traction-stretching curve for the springs

Because there is little test data for debonding strengths and fracture energies of 2D triaxial braided textile materials, and testing for this data is beyond the scope of the project, values used in the analyses are based on those used for unidirectional graphite epoxy composite laminates in Ref. 6. Values used for the three interfacial strengths T_i^c, $i = 1, 2, 3$, and the three critical strain energy release rates G_{Ic}, G_{IIc}, G_{IIIc} are listed in Table 3.

Table 3. Interfacial Strengths and Fracture Energies from Ref. 6

T_1^c, T_2^c	T_3^c	G_{Ic}	G_{IIc}, G_{IIIc}
11.6 ksi	8.7 ksi	2.01 lbs/in	8.28 lbs/in

Results

Refinements in the forty-eight degree frame model were required to capture the delamination process in the outer flange. To keep the model of reasonable size for the computational resources available, the model size had to be decreased for the smaller elements required to model decohesion associated with delamination. Using symmetry, only half of the frame was modeled. Boundary conditions modeling symmetry were used at the midspan location. With the physical model size decreased, the element size was reduced so that the smallest element in the outer flange was on the order of 0.06 inches (~1.6 mm). The model consisted of S4R shell elements, R3D8 rigid elements for the platen in the contact analysis, and the user-defined interface elements. The final model contained 16,770 elements and 15,081 nodes. However, ABAQUS then created 2,268 additional elements and 6,195 additional nodes of it's own to run the contact analysis.

Interface elements are only included in the midplane of the outer flange over a ten degree arc beginning at the midspan because of modeling difficulties and size limitations. Hence, the model cannot represent crack propagation from the outer flange into the web at the apex of the frame. Intralaminar progressive failure prediction is included for the shell elements making up the outer and inner sublayers of the outer flange surrounding the interface elements, and for the elements comprising the central span of the web and a section of the inner flange near the clamped end. This analysis captured the load-shortening response behavior fairly well with a large load drop followed by reloading as is shown in the load-deflection plot of Figure 5. The slope of the reloading portion of the response from FEA is within 10% of the test data at reloading. The energy absorbed predicted by the FEA is 11% lower than measured by the test, where the energy absorbed is the area under the load-deflection plot.

Along with the good correlation of the load-deflection behavior, the location of element failures correlate well with the locations of failure observed in the test. A comparison of the failed frame and the predicted element failures is shown in Figure 6. Failures observed during the test of frame *B* included the separation of the axial filler material in the outer flange at the apex of the frame, cracking of the front and back sides of the outer flange, and cracking of the web from the outer to the inner flange. Delamination and intralaminar element failures were predicted at the apex of the frame over the junction between the web and outer flange. Intralaminar failures were predicted in the back side outer flange and the web near the apex. The failure pattern and sequence predicted by the progressive failure model correlated very well with damage observed during the failure of frame *B* as reported in Ref. 3.

Concluding Remark

Including both interlaminar and intralaminar progressive failure models, geometric nonlinearity, and the contact of the platen with the frame in the ABAQUS finite element analysis resulted in very good correlation between the analysis and test through several major failure events of frame *B*.

References

[1]Pérez, José G., Richard L. Boitnott, and Eric R. Johnson, "Tests of Braided Composite Fuselage Frames Under Radial Inward Load," *The 41st AIAA/ASME/ASCE/AHS/A SC Structures, Structural Dynamics, and Materials Conference and Exhibit*, (Atlanta Georgia, April 3-6, 2000), Compact Disk, American Institute of Aeronautics and Astronautics, Reston, VA, 2000, (AIAA Paper No. 2000-1547)

[2]Naik, R. A., "TEXCAD - Textile Composite Analysis for Design: Version 1.0 User's Manual", NASA CR-4639, National Aeronautics and Space Administration, Hampton, Virginia, 1994.

[3]Pérez, José G., "Energy Absorption and Progressive Failure Response of Composite Fuselage Frames," Master of Science Thesis in Aerospace Engineering, Virginia Polytechnic Institute and State University, Blacksburg, VA 24061, July 1999.

[4]ABAQUS/Standard, Hibbitt, Karlsson, & Sorensen, Inc., 1080 Main St., Pawtucket, Rhode Island, 2001.

[5]Dávila, Carlos G., Ambur, Damodar R., McGowan, David M., "Analytical Prediction of Damage Growth in Notched Composite Panels Loaded in Axial Compression", *Proceedings of The 40th AIAA/ASME/ASCE/AHS Structures, Structural Dynamics and Materials Conference*, American Institute of Aeronautics and Astronautics, Reston, VA, 1999 (St. Louis MO) AIAA Paper No. 99-1435

[6]Goyal, V., Johnson, E.R., Dávila, C., and Jaunky, N., "An Irreversible Constitutive Law for Modeling the Delamination Process Using Interface Elements," *43rd AIAA/ASME/ASCE/ASC Structures, Structural Dynamics, and Materials Conference Proceedings on Disc [CD-ROM]*, American Institute of Aeronautics and Astronautics, Reston, VA, 2002, (Denver CO) AIAA Paper No. 2002-1576.

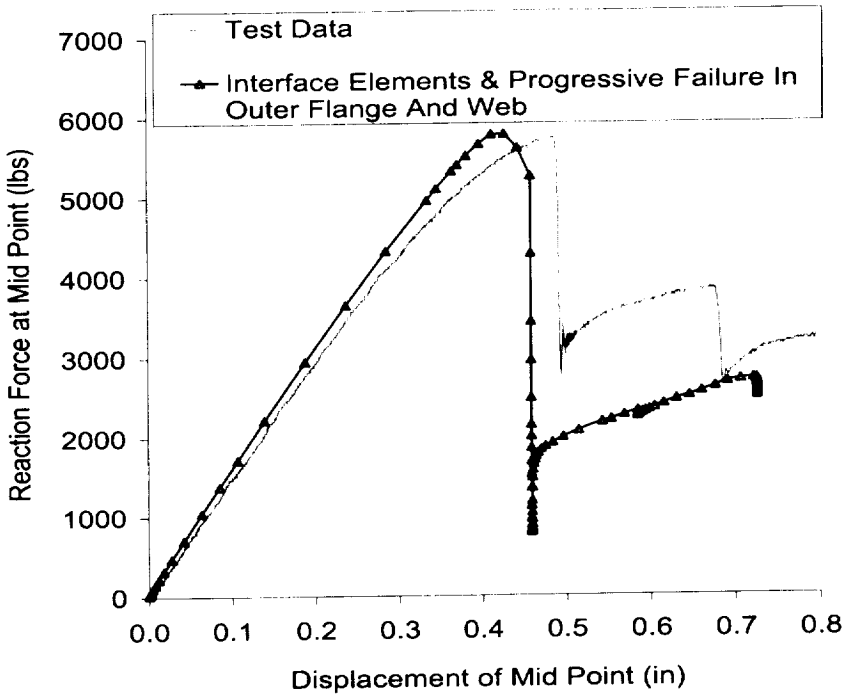

Figure 5 Load displacement responses from the analysis including both the intra- and interlaminar progressive failure models and the test. The domain of the intralaminar failure extended to web and inner flange.

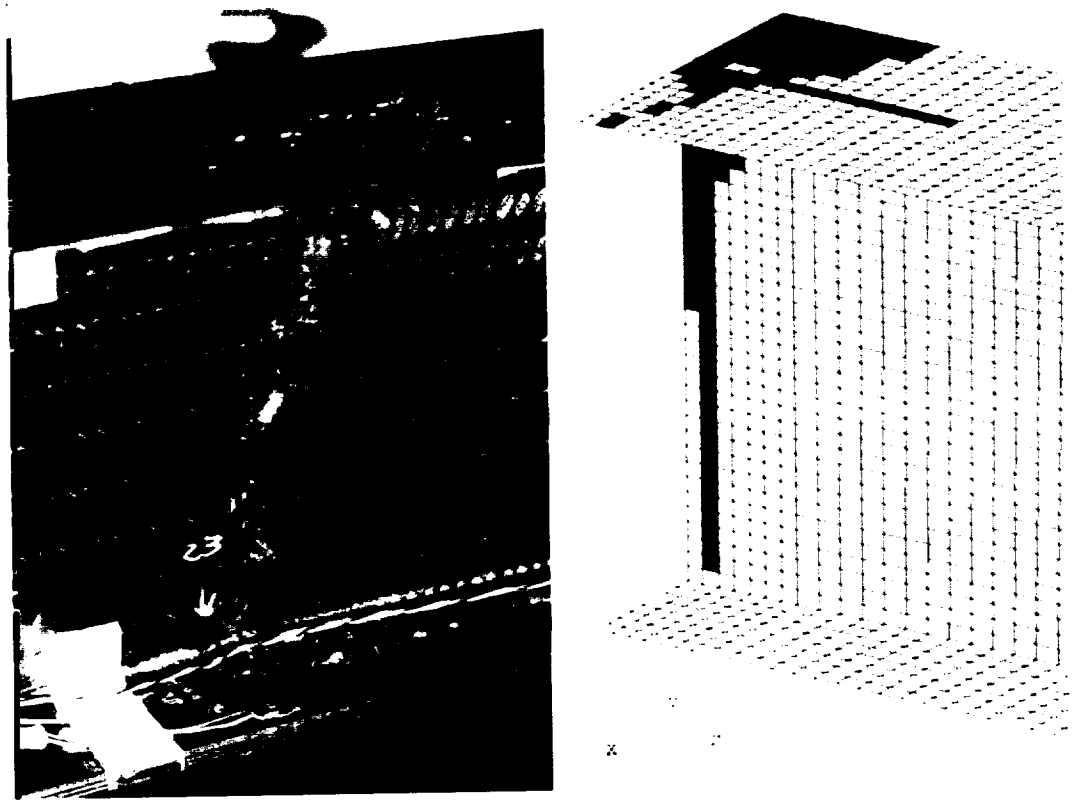

Figure 6 Comparison of the element failures predicted by the progressive failure model and failures that occurred on frame *B*.

Publications Supported by the Grant

Hart, D., Johnson, E.R., and Boitnott, R., "Response and Failure of Textile Composite Fuselage Frames Under Radial Inward Load," *43rd AIAA/ASME/ASCE/ASC Structures, Structural Dynamics, and Materials Conference Proceedings on Disc [CD-ROM]*, American Institute of Aeronautics and Astronautics (AIAA), Reston, VA, 2002, AIAA Paper No. 2002-1331.

Hart, Daniel C., "Development of a Progressive Failure Finite Element Analysis for a Braided Composite Fuselage Frame," Master of Science Thesis in Aerospace Engineering, Virginia Polytechnic Institute and State University, Blacksburg, VA 24061, July 2002.

Graduate Student Supported by the Grant

Daniel C. Hart, Master of Science in Aerospace Engineering, July 2002.